Ceramics International 44 (2018) 20019–20027

Contents lists available at ScienceDirect

Ceramics International

journal homepage: www.elsevier.com/locate/ceramint

New sintered wollastonite glass-ceramic for biomedical applications

Viviane O. Soares[a,1], Juliana K.M.B. Daguano[b], Christiane B. Lombello[b], Olavo S. Bianchin[c,2], Lívia M.G. Gonçalves[c,2], Edgar D. Zanotto[c,2]

[a] Departamento de Ciências, Universidade Estadual de Maringá, Goioerê, PR CEP 87360-000, Brazil
[b] Centro de Engenharia, Modelagem e Ciências Sociais Aplicadas, Universidade Federal do ABC (CECS / UFABC), São Bernardo do Campo, SP CEP: 09606-070, Brazil
[c] Laboratório de Materiais Vítreos, Departamento de Engenharia de Materiais, Universidade Federal de São Carlos (LaMaV-DEMa/UFSCar) - Center for Research, Technology and Education in Vitreous Materials, São Carlos, SP CEP:13565-905, Brazil

ARTICLE INFO

Keywords:
A. Sintering
D. Glass-ceramics
C. Mechanical properties
E. Biomedical

ABSTRACT

We developed a new bioactive glass-ceramic (GC) based on the CaO-SiO_2-MgO-Na_2O-Li_2O system. Four glass compositions were formulated by a proprietary software (Reformix) and tested by changing mainly the calcium content (from 20 mol% to 40 mol%) and the minor components - alumina, zirconia and zinc oxide. We produced our GCs using the sinter-crystallization process at different temperatures (800–1000 °C) and evaluated the effects of compositional changes on the sintering kinetics, microstructure (residual porosity and crystalline phases), hardness, bending strength and bioactivity. We then followed the hydroxycarbonate apatite (HCA) formation in simulated body fluid by Fourier-transform infrared spectroscopy (FTIR), which revealed the onset of HCA formation after approximately 3 days. These GCs are phosphorus and fluorine free, elements that are present in most bioactive glasses, glass-ceramics and ceramics. Our most bioactive GC has a residual porosity of 9 ± 1%, hardness of 5.5 ± 0.3 GPa, 4p-bending strength of 98 ± 7 MPa and is non-cytotoxic. This combination of good bioactivity and mechanical properties (despite its high porosity) suggests that this new GC could be tested for bone graft implants.

1. Introduction

Ca-rich silicate glass-ceramics (GCs) containing wollastonite ($CaSiO_3$) crystals have received a great deal of attention due to their good bioactivity, biocompatibility and mechanical properties [1–3]. These GCs enhance bone regeneration and can be applied in bone tissue engineering. The wollastonite crystalline phase often presents acicular morphology, which potentially increases the GC´s toughness and strength [4].

Sintering is the most common route for the production of wollastonite GCs due to the preferential surface (rather than volume) crystallization of the related glass forming system, CaO-MgO-SiO_2-P_2O_5 [1]. During the sintering process, concurrent crystallization - induced by surface defects - takes place on the rough glass particles that are created during the milling procedure [5] or on solid impurity particles existing on the surfaces.

The classical Cerabone® A-W GC is produced by sintering with concurrent crystallization and has about 38 wt% apatite, 34 wt% β-wollastonite and 28 wt% residual glass phase. This combination of two crystalline phases and the residual glass (estimated to have 16.6 wt% MgO, 24.2 wt% CaO and 59.2 wt% SiO_2) shows a moderate bioactivity level (bioactivity index $I_B = 3.2$) [6]. The surface of Cerabone® A-W GC becomes completely covered with an apatite layer after a 7-day immersion in simulated body fluid (SBF) and its capacity to glue to bony tissue is attributed to this layer [7]. The reported 3p-bending strength of this GC is about 215 MPa, which is higher than the typical 160 MPa of human cortical bone. This is attributed to the precipitation of β-wollastonite needles, as well as apatite [7]. Cerabone® A-W GCs have been successfully used in more than 60,000 clinical cases, including iliac crest vertebral replacement and repair [8].

Sintering of glass particles with concurrent crystallization is thus a viable alternative route to produce GCs. The advantage of this process is that the high specific surface area of fine ground glass powders promotes surface crystallization even without adding any nucleating agent [9,10]. However, if the surface crystallization process is too fast, crystals develop and cover the particle surfaces prior to full densification,

E-mail address: vosoares@uem.br (V.O. Soares).
[1] Postal address: Avenida Reitor Zeferino Vaz, s/n, Jardim Universitário, Goioerê, Paraná CEP 87360-000, Brazil.
[2] www.certev.ufscar.br.

https://doi.org/10.1016/j.ceramint.2018.07.275
Received 15 May 2018; Received in revised form 10 July 2018; Accepted 30 July 2018
Available online 02 August 2018

then sintering by viscous flow is hindered [11]. The crystallized surfaces of the particles do not flow, thus stopping the sintering process [12,13]. This is the main cause of residual porosity in most sintered GCs.

The purpose of the present study was to investigate the *sinter-crystallization* process of four glass compositions in the CaO-MgO-SiO_2 system, which were designed to present high sinterability and to correlate the formed microstructures with some *mechanical properties* (hardness and strength) and bioactivity (HCA layer formation in SBF). The final objective was to develop a new, strong and bioactive GC.

2. Materials and methods

2.1. Glass preparation and milling

The glass compositions were based on the CaO-SiO_2-MgO-Na_2O system and designed using the proprietary software Reformix 2.0 (LaMaV-UFSCar, Brazil) and the Sciglass® database (ITC Inc.). These glasses are phosphorus and fluorine free, and were labeled using the following convention: xCa, x = 40, 30, and 20 mol% of CaO. The nominal compositions of the 40Ca, 30Ca, 20Ca and 20CaII glasses (mol %) are shown in Table 1. The levels of Na_2O, Li_2O and ZnO were varied in each composition to improve bioactivity, whereas the 30Ca and 20Ca compositions were developed aiming to improve the sintering of these glasses. MgO and Al_2O_3 were added to increase the surface tension of the glasses and consequently improve viscous flow sintering [10,14]. ZrO_2 was used to improve the glass forming ability and thus prevent devitrification during the casting of relatively large pieces. As reported in the literature, ZrO_2 acts as network intermediate, and can be a network former in silicate glasses having low ZrO_2 concentration [15,16].

We used analytical grade oxides and carbonates (SiO_2, $CaCO_3$, Al_2O, ZrO_2, MgO, Li_2CO_3, Na_2CO_3 and ZnO). The proper mixtures of these reagents were homogenized in a planetary ball mill (Fritsch, model Pulverisette 5) at 300 rpm for 15 min, using an agate jar and 18 agate balls of 20 mm in diameter. The glasses were melted in an electrical furnace at atmospheric pressure at 1400 °C for 4 h in a platinum crucible. The melts were poured on a stainless steel plate and pressed with a stainless steel plaque every 1 h. They were then crushed and re-melted over a total of three re-melting procedures to ensure homogeneity.

The obtained glasses were milled in a planetary ball mill (Fritsch, Pulverisette 5) in an agate jar using 18 agate balls of 20 mm in diameter at 450 rpm for 60 min. The resulting glass particle size distribution was measured by a laser diffraction particle size analyzer (Horiba, model LA930).

The characteristic temperatures of the glass powders (T_g - glass transition and T_x - the onset of the crystallization peaks) were determined by Differential Scanning Calorimetry, (DSC) (Netzsch, model STA 404) using a heating rate of 20 °C min^{-1} and a temperature range from 50 °C to 1100 °C.

Table 1
Chemical compositions of the investigated glasses (mol%).

Glass Composition	40Ca	30Ca	20Ca	20CaII
CaO	40.0	31.6	20.0	22.0
SiO_2	52.0	49.7	53.3	55.3
MgO	3.0	9.0	10.0	12.0
Al_2O_3	0.4	3.0	3.0	–
ZrO_2	–	5.0	5.0	–
Li_2O	0.5	1.7	1.7	1.7
Na_2O	–	–	7.0	9.0
ZnO	2.7	–	–	–
Other	1.5	–	–	–

2.2. Sintering

A heating stage microscope (HSM) (Expert system solutions, model Misura HSM ODHT) was used to follow the sintering behavior of each composition. This technique allows the quantification of the sample shrinkage during heating by measuring the variation of its dimensions. A constant heating rate of 20 °C/min was used to compare HSM results to DSC curves. A cylindrical compact of glass particles (3.2 mm (diameter) by 4.8 mm (height)) was placed on an alumina support and the temperature was measured using a platinum-rhodium thermocouple under the support. The heating microscope projected the image of the sample through a quartz window and the images were captured by a video camera during the heating ramp every 2 °C. The linear shrinkage of the sample (height) as a function of temperature was determined and compared to the respective DSC curve of each glass. This experiment was carried out to evaluate the effect of compositional changes on the sinterability of the GCs.

Glass powders were compacted into a cylindrical shape (10 mm in diameter and 4 mm in height) under a uniaxial pressure of 130 MPa for 30 s. Glass compacts were then sintered at temperatures ranging from 800° to 1000°C, using a heating rate of 30 °C/min without any holding time. The samples were cooled inside the furnace at approximately 15 °C/min. The samples were sintered in a temperature interval in which no more shrinkage was observed to ensure maximum densification and subsequent crystallization, since crystallization was desired.

After sintering, the samples were ground with SiC abrasive paper and polished in a suspension of CeO_2. The porosity of the sintered samples was determined by optical microscopy (Leica, model DM-RX with a CCD camera DFC 490) and image analysis using the ImageJ software.

The crystalline phases formed in GCs were determined by X-ray diffraction (XRD) using a Rigaku Ultima IV diffractometer, with Cu-Kα radiation in the 2θ range from 20 ° to 70 ° using continuous scans at 2 °/min. The crystallized volume fraction in the GCs was estimated according to the procedure used by Krimm and Tobolsky [17]. The percent crystallinity (*IC*) was calculated by the ratio of the crystalline area (A_C) and the total area (A_T, where A_T = amorphous + crystalline), present in the GC diffractograms, using the following equation [18]:

$$IC = (A_C/A_T) \text{ x } 100 \quad (1)$$

The content of vitreous phase (%) was then 100 - *IC*.

Scanning electron microscopy (SEM – Philips, model XL-30 FEG) was used to observe the microstructure of polished and etched (by immersion in 0.2 vol% HF for 10 s) transversal sections of samples coated with a thin layer of gold.

2.3. Mechanical properties

The hardness and indentation toughness (K_c) of the GCs were measured using a microindentator Vickers (Zwick/Roell, model Indentec ZHV) with an applied load of 2.94 N for 15 s. For reasonable statistics, at least 10 Vickers impressions were made on the polished surface of each sample. The elastic modulus (*E*) was measured by instrumented nanoindentation (MTS, model Nanoindenter XP) using the Oliver and Pharr method [19] with a Berkovich diamond indenter. The maximum load was 400 mN. Each data point was calculated from the average of at least nine indentations.

The flexural strength (σ_f) was measured for each GC composition. A four-point bending setup (Instron, model 5569) with an outer span of 30 mm and an inner span of 10 mm at a crosshead speed of 0.1 mm/minute was used. Six bars of 9 × 4 × 42 mm^3 for each condition were used for the bending tests. The sample surfaces were polished using a CeO_2 solution. This test was performed according to ASTM C158-84 [20].

2.4. In vitro bioactivity tests in SBF

The in vitro bioactivity of the GCs was investigated according to the method described by Kokubo et al. [21] by immersing cylindrical samples in SBF (simulated body fluid) at 37 ± 0.1 °C. SBF is an acellular, protein-free solution with an ionic concentration (in mM) of 142.0 Na^+, 5.0 K^+, 2.5 Ca^{2+}, 1.5 Mg^{2+}, 147.8 Cl^-, 4.2 HCO^{3-}, 1.0 HPO_4^{2-} and 0.5 SO_4^{2-}, buffered at pH 7.25 with tris-hydroxymethyl-aminomethane (Tris, 50 mM) and hydrochloric acid solutions.

During the tests, the samples were in contact with the SBF solution for 0, 3, 7, 10 and 14 days. After each test time, they were removed from the bottles and immersed in acetone for 10 s to remove the excess SBF and stop the surface reactions. After drying, both sample surfaces were analyzed to check for the formation of an HCA layer. After the in vitro bioactivity tests were conducted, the surface modifications of the samples were monitored by Fourier transform infrared spectroscopy (FTIR) using a PerkinElmer, Spectrum GX model spectrometer operating in reflectance mode with a 4 cm^{-1} resolution in the 4000–400 cm^{-1} region.

2.5. In vitro cytotoxicity tests

The cytotoxicity tests were conducted according to the ISO 10993-5 standard [22], applying the elution technique. The GC samples were incubated in culture medium (199 medium, with 10% fetal calf serum) for 48 h at 37 °C. Vero cells were inoculated in 24 wells culture plates at 10^5 cells/ml. The cells were incubated with culture medium (199 medium with 10% fetal calf serum) at 37 °C and 5% CO_2. After 24 h, sub-confluent cell culture substrates were obtained and the culture medium was changed for the elution medium of each biomaterial. The negative control was the culture medium only, and the positive medium was a 0.25% phenol solution. After 24 h, the cells were observed in an inverted microscope with phase contrast (Zeiss, model Axio Vert. A1). The cells were fixated with glutaraldehyde 2.5% and stained with Toluidine Blue.

3. Results

The particle size distributions (PSD) obtained for each glass are shown in Fig. 1. Glasses 40Ca and 30Ca show a similar PSD, with an average particle size of approximately 3 μm. For 20Ca and 20CaII, the average particle sizes are 7 μm and 14 μm, respectively, and they have a broader PSD.

We investigated the sintering behavior of the glasses by combining DSC and HSM to find the most appropriate sintering temperature range for each composition (Fig. 2). Table 2 reports the characteristic temperatures (T_g and T_c), the sintering window (T_c-T_g) of 40Ca, 30Ca, 20Ca and 20CaII, determined from their DSC curves, and the sintering temperatures (T_{sint} and T_{sat}), obtained by an HSM. The temperature at

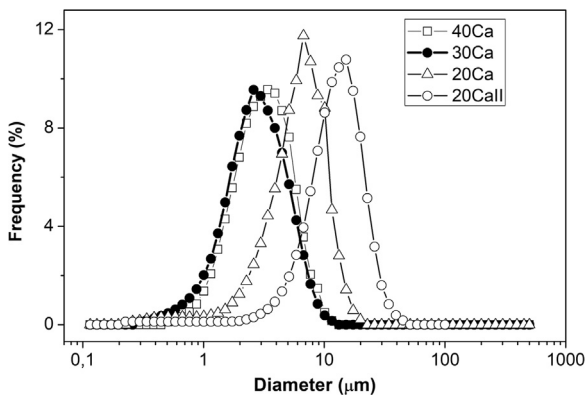

Fig. 1. Particle size distributions of the glass powders used here.

which sintering starts (T_{sint}) was considered to correspond to the first 1% in linear retraction, and T_{sat} is the temperature for sintering saturation.

Fig. 2(a) shows that T_{sat} (850 °C) is close to T_x (860 °C) for composition 40Ca. The shrinkage of the sample stops when crystallization starts. The sintering temperatures adopted for this composition were 900 °C, 950 °C and 1000 °C to promote the sample crystallization after sintering. As shown by Fig. 2(b), composition 30Ca shows a reduction in the sintering rate (defined as dH/dT, where H is the height of the sample and T is temperature) at 830 °C. This sample continued to shrink even after the beginning of crystallization (T_x), indicated by the first exothermic peak determined by DSC analysis. Sintering and crystallization are concurrent processes up to approximately 900 °C. This glass presents two exothermic peaks, which suggests the formation of at least two crystalline phases. The sintering temperatures adopted were 950 °C and 1000 °C. Glass 20Ca also undergoes simultaneous sintering and crystallization in the temperature range of 832–874 °C, as shown in Fig. 2(c). The sintering temperatures adopted were 850 °C, 900 °C, 950 °C and 1000 °C. Fig. 2(d) shows that the 20CaII composition presents a change in the sintering rate at 700 °C and the sintering and crystallization are concurrent processes from 770 °C (T_x) up to 814 °C (T_{sat}). This composition was sintered at 800 °C, 850 °C and 900 °C.

The porosity (p) as a function of sintering temperature, with a heating rate of 30 °C/min, is shown in Fig. 3. The sintering temperature that leads to the minimum residual porosity for GC 40Ca is 950 °C (p = 3.7 ± 0.2%), and for GC 30Ca it is 1000 °C (p = 0.4 ± 0.1%), although a small difference was observed in porosity for the same composition. For GC 20Ca and GC 20CaII, the maximum densification was reached at 850 °C (p = 0.7 ± 0.1%) and 800 °C (p = 5.9 ± 0.8%), respectively. We observed that for GC 20Ca and GC 20CaII, the porosity increases with the increasing sintering temperature. The porosity of Cerabone® A-W was also measured by the same method and it is 5.0 ± 0.3%.

XRD patterns of sintered GCs are shown in Fig. 4. The crystalline phases present in the GC 40Ca are $CaSiO_3$ (wollastonite 2 M) and SiO_2 (quartz), Fig. 4(a). The higher intensity of SiO_2 peaks for the GC sintered at 1000 °C indicates that the crystallization of wollastonite occurs at lower temperatures, and then the silica-rich residual glass allows for the precipitation of quartz. As can be seen in Fig. 4(b), $MgCaSiO_6$ (diopside) and $CaSiO_3$ (wollastonite 1 A) are the crystalline phases present in GCs 30Ca for both sintering temperatures. Fig. 4(c) shows the XRD pattern for GCs 20Ca sintered at 900 °C and 950 °C. At 900 °C only diopside is crystallized and a background is observed which indicates a significant amount of residual vitreous phase in this sample. At 950 °C, the crystalline phases identified were $MgCaSiO_6$ (diopside), $CaSiO_3$ (Parawollastonite) and $ZrSiO_4$ (zirconium orthosilicate). The sintering temperature of 950 °C was adopted as the best sintering condition for GC 20Ca due to its higher crystallization. As shown in Fig. 4(d), GCs 20CaII presents diopside as the main phase, $Na_{4.2}Ca_{2.8}(Si_6O_{18})$ (combeite) and few peaks of $CaSiO_3$ (β-Wollastonite) for both sintering temperatures. GC 20CaII sintered at 800 °C shows low intensity XRD peaks, which indicates a higher content of vitreous phase in this sample, hence we adopted 850 °C as the best sintering condition to favor crystallization avoiding significantly reducing densification (see Fig. 3).

An XRD pattern of the commercial Cerabone® A-W GC is shown in Fig. 5. Two major crystalline phases, $CaSiO_3$ (wollastonite) and $Ca_{10}(PO_4)_6(OH,F_2)$ (hydroxylfluoroxyapatite) were identified in this material. These findings agree with the results published by Kokubo. According to that author, the commercial GC Cerabone® A-W with a nominal composition MgO 4.6, CaO 44.7, SiO_2 34.0, P_2O_5 16.2, CaF_2 0.5 wt% heat-treated at 1050 °C presents 38 wt% of $Ca_{10}(PO_4)_6(O,F_2)$ (oxyfluorapatite) and 34 wt% of $CaSiO_3$ (β-wollastonite) [4].

Fig. 6 shows the microstructure of sintered GC 40Ca at 1000 °C, GC 30Ca at 950 °C, GC 20Ca at 950 °C, GC 20CaII at 850 °C and Cerabone® A-W, respectively. GC 40Ca presents a high crystallized fraction and crystal size under 5 μm, as can be seen in Fig. 6(a). GC 30Ca shows

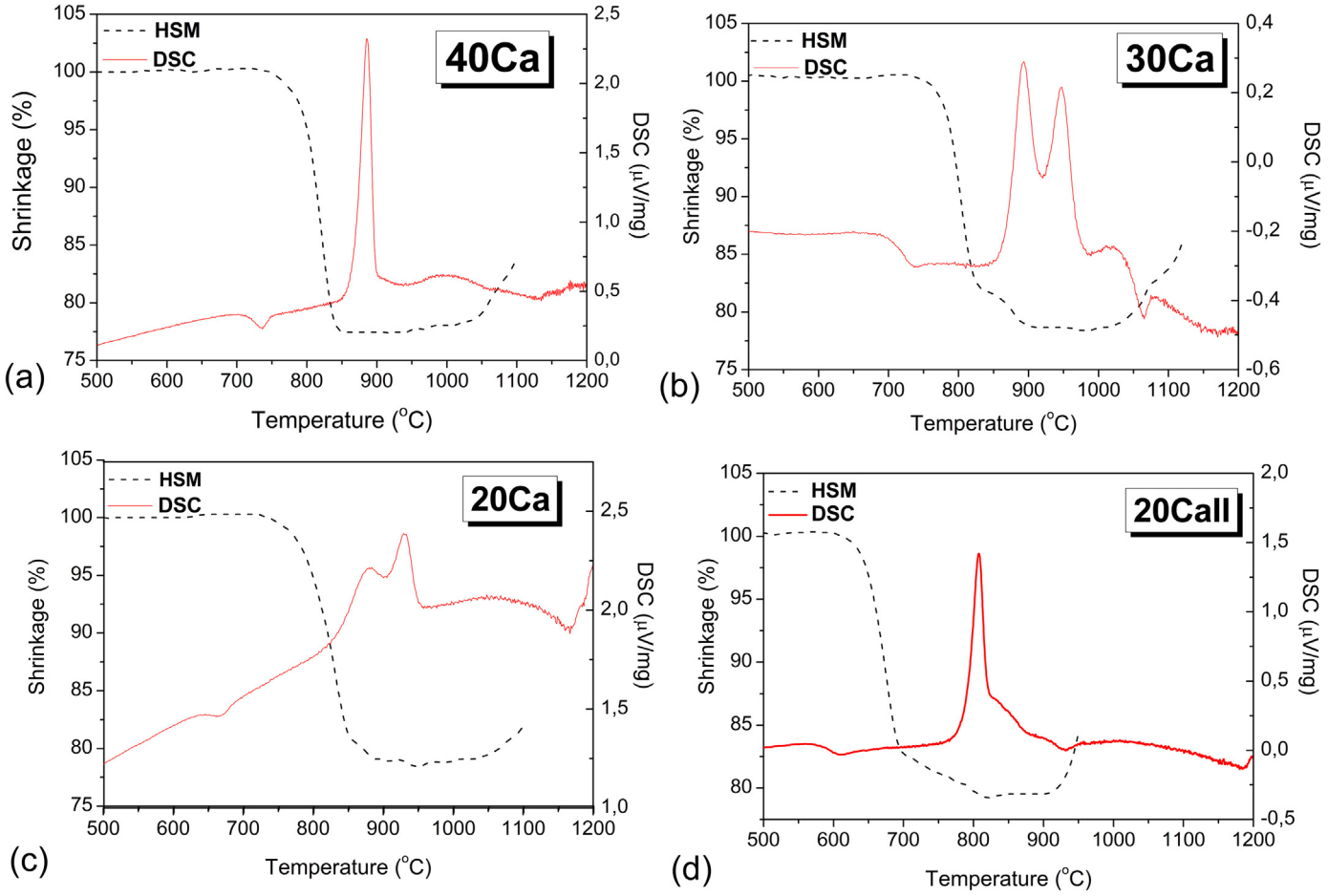

Fig. 2. Linear shrinkage (H) as a function of temperature obtained by HSM compared to DSC analysis, using a heating rate of 20 °C/min: (a) 40Ca, (b) G30Ca, (c) 20Ca, (d) 20CaII.

Table 2
Characteristic temperatures and sintering window (T_x-T_g) of the 4 glass compositions used here.

Composition	T_g (°C)	T_x (°C)	T_{sint} (°C)	T_{sat} (°C)	T_x-T_g (°C)
40Ca	709	860	780	850	151
30Ca	694	862	778	890	168
20Ca	638	832	770	874	194
20CaII	580	770	640	814	190

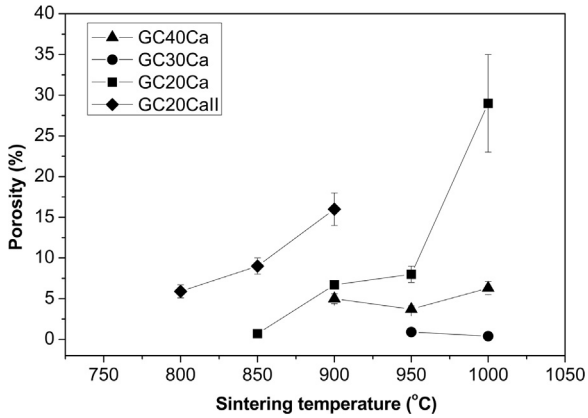

Fig. 3. Porosity as a function of sintering temperature for all compositions.

interconnected crystals with an average size under 5 μm and a vitreous phase surrounding them (Fig. 6(b)). GC 20Ca presents two crystal morphologies: acicular and small squares, the acicular crystals were removed by etching and the squares are surrounding by a vitreous phase (Fig. 6c). G20 CaII presents acicular crystals having a crystal size up to 20 μm, some pores and vitreous phase are also observed (Fig. 6(d)). Cerabone® A-W microstructure is shown in (Fig. 6(e)), where crystals with a medium size under 1 μm can be seen.

Table 3 shows the values of porosity, percentage of vitreous phase, hardness, and bending strength (σ_f) obtained for GCs 40Ca, 30Ca, 20Ca and 20CaII sintered at different temperatures and the commercial Cerabone® A-W.

Table 3 shows that the percentage of the vitreous phase decreases with increasing sintering temperature, as expected. Except for GC 30Ca, the increase in the vitreous phase in the sample sintered at 1000 °C, when compared to that sintered at 950 °C, is probably due to the melting peak observed in the DSC curve at around 1035 °C (Fig. 2(b)). The percentages of the residual vitreous phase identified for all the GCs developed in this work vary from 18% to 37%. It is important to note that the fraction of vitreous phase identified here for Cerabone® A-W is equal to the value reported in the literature (28%) [4].

The hardness of the developed GCs varies from 5.5 to 7.7 GPa; GCs 30Ca and 20Ca, which contain Al_2O_3 and ZrO_2, have a relatively higher hardness, as expected. In contrast, GCs 20CaII have the lowest values of hardness, and no significant difference in hardness when compared to the glass 20CaII. GC 30 Ca sintered at 1000 °C and GC 20Ca sintered at 900 °C present the lowest flexural strength (64 ± 3 MPa and 74 ± 6 MPa, respectively) of these GCs compared to GC 40Ca and GC 20CaII (98 MPa).

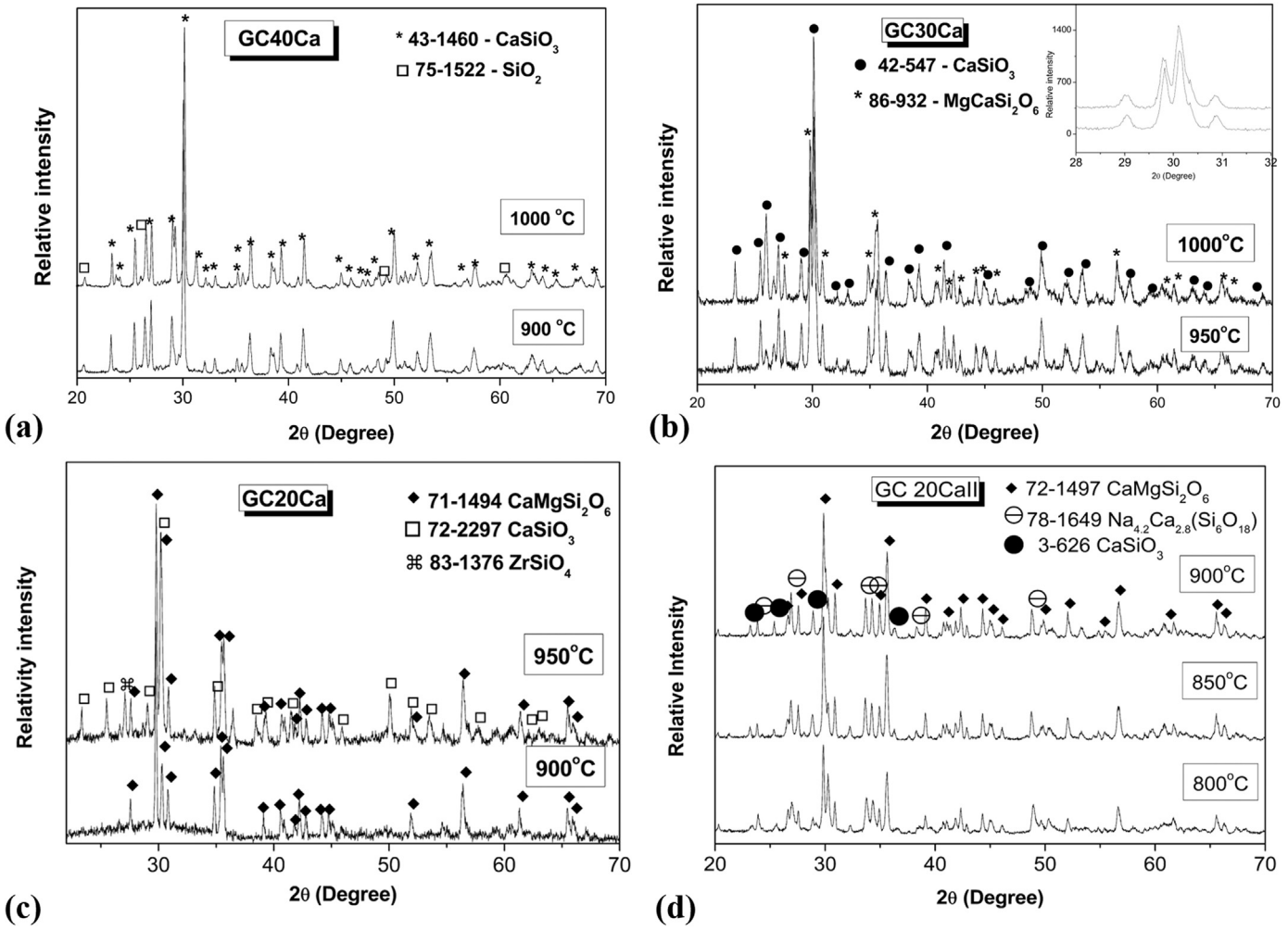

Fig. 4. XRD patterns of our glass-ceramics: (a) GC40Ca, (b) GC30Ca, (c) GC20Ca, (d) GC20CaII sintered at different temperatures.

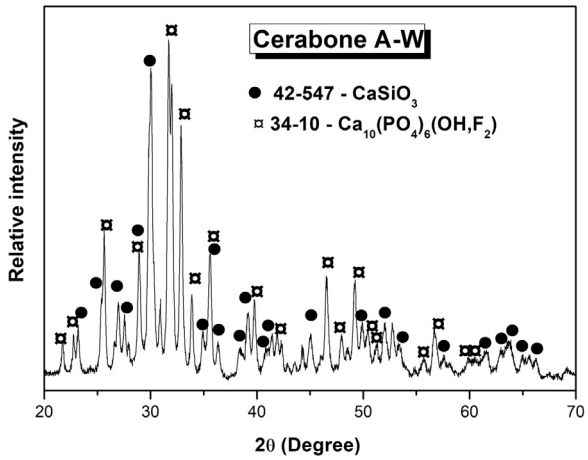

Fig. 5. XRD pattern of the Cerabone® A-W glass-ceramic.

The FTIR spectra for the GCs before and after immersion in SBF up to 7 days are shown in Fig. 7. The bioactivity test was performed only in the samples previously tested for flexural strength.

Fig. 7(a) shows that the GC 20CaII sintered at 850 °C presents the formation of HCA after 3 days. It is characterized by the appearance of the double peak from P–$O_{(b)}$ bonds at 565 cm^{-1} and 605 cm^{-1}, the peak from the stretching of the P–$O_{(s)}$ bonds at 1050 cm^{-1} and by the peak from P = $O_{(s)}$ bonds at 1120 cm^{-1}.

For the other GCs, the formation of HCA was not identified because it is not possible to note significant variations in the spectra obtained before and after immersion in SBF, even for periods up to 7 days (Fig. 7(a)). It is believed that this behavior is consistent with an inert material, i.e. a material which when in contact with body fluids has a low interaction due to the higher chemical durability.

The difference in the reactivity of the precursor glass 20CaII and the GC 20CaII is shown in Fig. 7(b) and it is represented by the time necessary for the beginning of HCA formation. As the 20 CaII is the only composition that resulted in a bioactive GC, the bioactivity test of the 20CaII glass is also shown in Fig. 7(b). Since the precursor 20CaII glass is not bioactive, the formation of crystalline phases during the sintering step are fundamental for obtaining the bioactive GC20CaII. Before immersion in SBF, GC 20CaII presents a FTIR spectrum different to that of glass 20CaII due to its high crystallized fraction. For the glass 20CaII, the HCA formation time exceeded 3 days, since no change was observed among spectral features before and after immersion in SBF, whereas for GC 20CaII, the bands referring to the HCA layer are already visible after 3 days, characterized by the bands mentioned above and also by the band at 890–850 cm^{-1} related to the C-$O_{(s)}$ bonds. Peitl et al. [23] observed the development of a HCA layer even in fully crystallized glass-ceramics obtained from glasses having a chemical composition between $1Na_2O$-$2CaO$-$3SiO_2$ and $1.5Na_2O$-$1.5CaO$-$3SiO_2$. They showed that the crystal phase $1Na_2O$-$2CaO$-$3SiO_2$ (and similar phases) has a high bioactive index and, consequently, crystallization does not affect much the bioactivity of highly crystallized GCs in that system.

Cerabone® A-W was chosen as a standard in this work because its

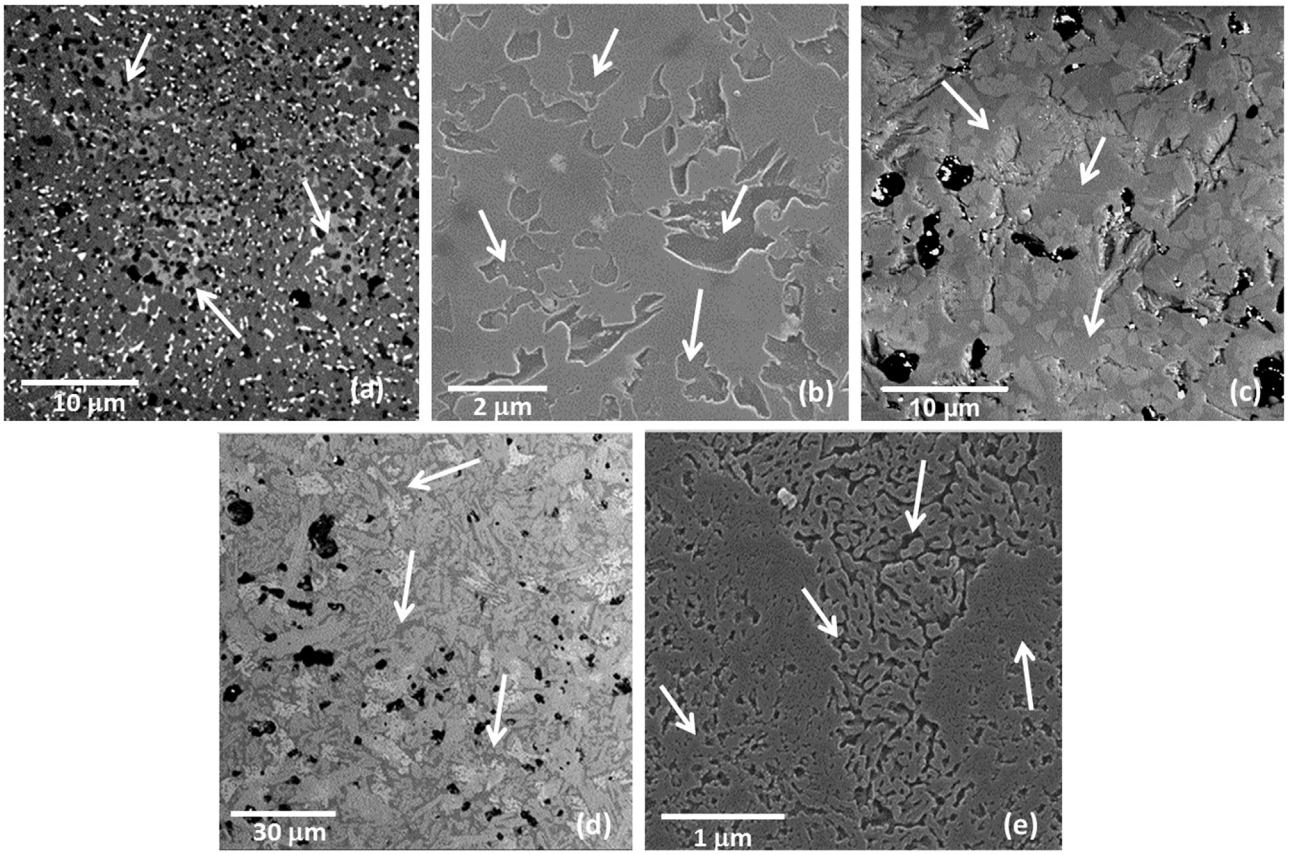

Fig. 6. SEM of sintered samples surfaces chemical etched in 0.2%vol. HF: (a) GC 40Ca sintered at 1000 °C, BSE detector; (b) GC 30Ca sintered at 1000 °C, SE detector; (c) GC 20Ca sintered at 900 °C, BSE detector; d) GC 20CaII sintered at 850 °C, BSE detector and (e) Cerabone® A-W, SE detector. White arrows indicate the residual vitreous phase.

Table 3
Porosity, vitreous phase content, hardness and 4p-bending strength (σ_f) for GCs 40Ca, 30Ca, 20Ca, 20CaII and Cerabone® A-W.

Composition (GC)	Sintering temperature (°C)	Porosity (%)	Vitreous phase (%)	Hardness (GPa)	σ_f (4-point) (MPa)
40Ca	1000	6.3 ± 0.8	21	5.9 ± 0.1	98 ± 6
	900	3.7 ± 0.4	30	6.7 ± 0 0.3	–
	Glass	–	–	6.6 ± 0.3	–
30Ca	1000	0.4 ± 0.1	37	6.9 ± 0.3	64 ± 3
	950	0.9 ± 0.3	18	7.3 ± 0.3	–
	Glass	–	–	7.3 ± 0.4	–
20Ca	950	8 ± 1	25	7.7 ± 0.8	–
	900	6.7 ± 0.5	36	7.1 ± 0.2	74 ± 6
	Glass	–	–	6.9 ± 0.2	–
20CaII	850	9 ± 1	19	5.5 ± 0.5	98 ± 7
	800	5.9 ± 0.8	24	5.7 ± 0.5	–
	Glass	–	–	6.5 ± 0.5	–
Cerabone® A-W	Commercial	5.0 ± 0.3	28	6.9 ± 0.3	215 (3-points)[a]

[a] Kokubo [4].

reactivity in SBF solution has been extensively studied. From Fig. 7(b), the formation of a HCA layer in AW Cerabone® A-W can be observed after 7 days, as indicated by the bands at 565–605 cm^{-1}, 1050 cm^{-1} and 1120 cm^{-1}. The time required for the formation of a HCA layer in Cerabone® A-W (7 days) is considerably higher when compared to GC 20CaII, which is 3 days.

Fig. 8 shows the cytotoxicity evaluation performed by the elution technique. Positive and negative controls were used to confirm the adequate performance of the test procedure and/or to evaluate the results from a new material, as well as to control cell sensitivity, extraction efficiency and other test parameters.

As shown in Fig. 8(a), the negative control showed a pattern of cell morphology and the positive control demonstrates lysed and degenerated cells (Fig. 8(b)). All the tested GCs were considered non-cytotoxic (Fig. 8(c); (d); (e) and (f)), because the morphology of the cells treated with the elution solution is similar to that of the negative control (Fig. 8(a)).

4. Discussion

The 30Ca, 20Ca and 20CaII glass compositions were developed from the 40Ca by reducing the calcium and increasing MgO, Na_2O, Al_2O and ZrO_2; the nominal compositions are shown in Table 1. These chemical changes induced modifications in the sinter-crystallization process. The 40Ca composition presents the highest temperatures T_g and T_{sint} (see Table 2), however it shows a high shrinkage prior to crystallization (Fig. 2a)). Moreover, the sintering process ends (T_{sat} = 850 °C) with the beginning of superficial crystallization of the particles (T_x = 860 °C). The intense crystallization peak hinders the sintering in this composition, which has a sintering window of only 151 °C.

For composition 30Ca, the reduction in CaO and increase in MgO, ZrO_2 and Al_2O_3 (see Table 1) decreased 15 °C in Tg (694 °C) without significant changes in T_x (862 °C) and, consequently this composition has a higher sintering window when compared to 40Ca (Table 2). The sintering process and crystallization occurs simultaneously in 30Ca, as can be seen in Fig. 2(b), the compact continues shrinking in temperatures higher than T_x, and as a consequence the GCs obtained from this composition show the lowest porosity ($p < 1\%$) (Fig. 3).

Composition 20Ca was developed based on 30Ca, reducing CaO,

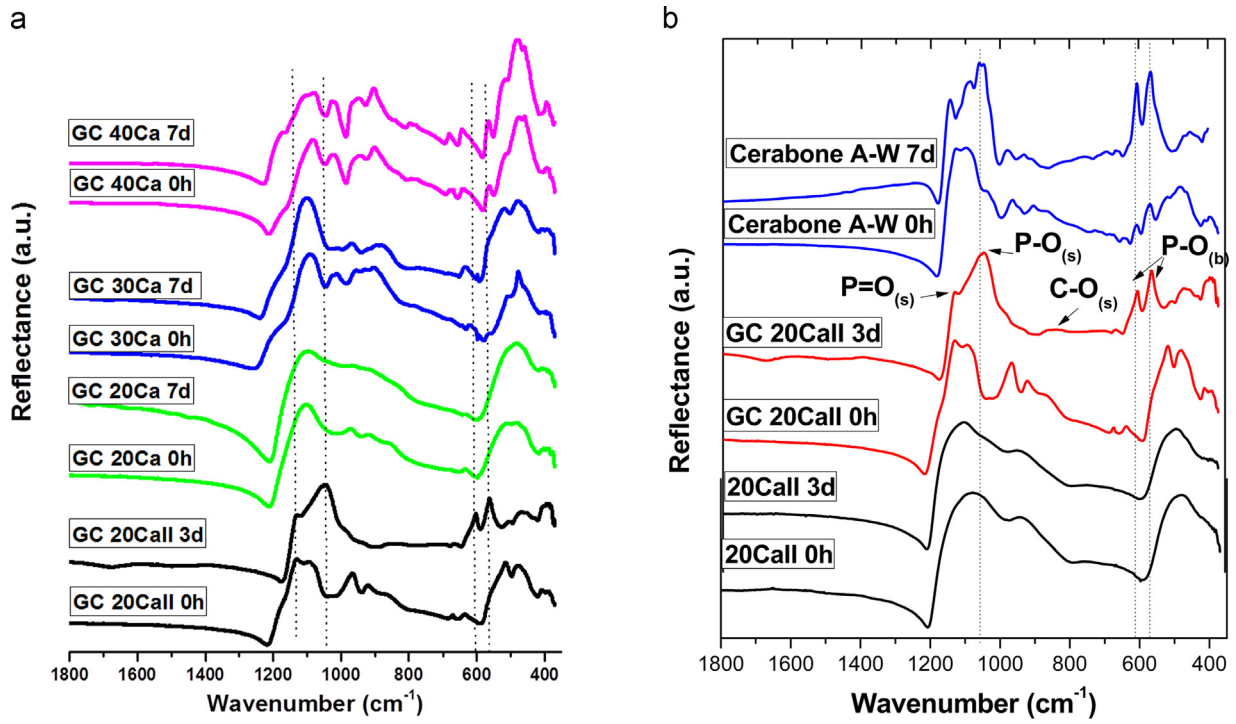

Fig. 7. FTIR spectra of sintered GCs: (a) GC 40Ca (1000 °C), GC 30Ca (1000 °C), GC 20Ca (900 °C) and GC 20CaII (850 °C) before (0 h) and after immersion in SBF up to 7 days; (b) glass 20CaII and GC 20CaII sintered at 850 °C, before and after immersion in SBF for up to 7 days. The spectrum for the standard Cerabone® A-W is also shown.

adding Na_2O and increasing MgO (see Table 1). As shown in Table 2, these changes in composition decreased T_g significantly (T_g = 638 °C and ΔT_g = 56 °C) and improved the sintering window (194 °C). However, as can be seen in Fig. 3, this composition presents an increase in porosity with the sintering temperature. This occurs due to degassing, as described in previous studies on other sintered GCs [5,12]. Therefore, for composition 20Ca, it is not possible to obtain a GC having a high crystallized fraction and low porosity due to the degassing increase with crystallization.

The 20CaII composition was based on 20Ca, where Al_2O_3 and ZrO_2 were removed and the other components (CaO, SiO_2, MgO and Na_2O) had an increase in 2 mol% (see Table 1). According to Table 2, these changes in the composition reduced 58 °C in T_g (580 °C) and 62 °C in T_x (770 °C) compared to 20Ca, which resulted in a similar sintering window (190 °C). A large sintering window (ideally around 200 °C [24]) improves densification and is necessary for several glass applications, such as the production of porous scaffolds. As can be seen in Fig. 3, this composition also presents degassing characterized by the increase in porosity with a sintering temperature. Despite this, 20CaII presented a good densification (p = 5.9 ± 0.8% at 800 °C) and is suitable for low temperature sinter-crystallization.

Other bioactive glass compositions have been designed with an

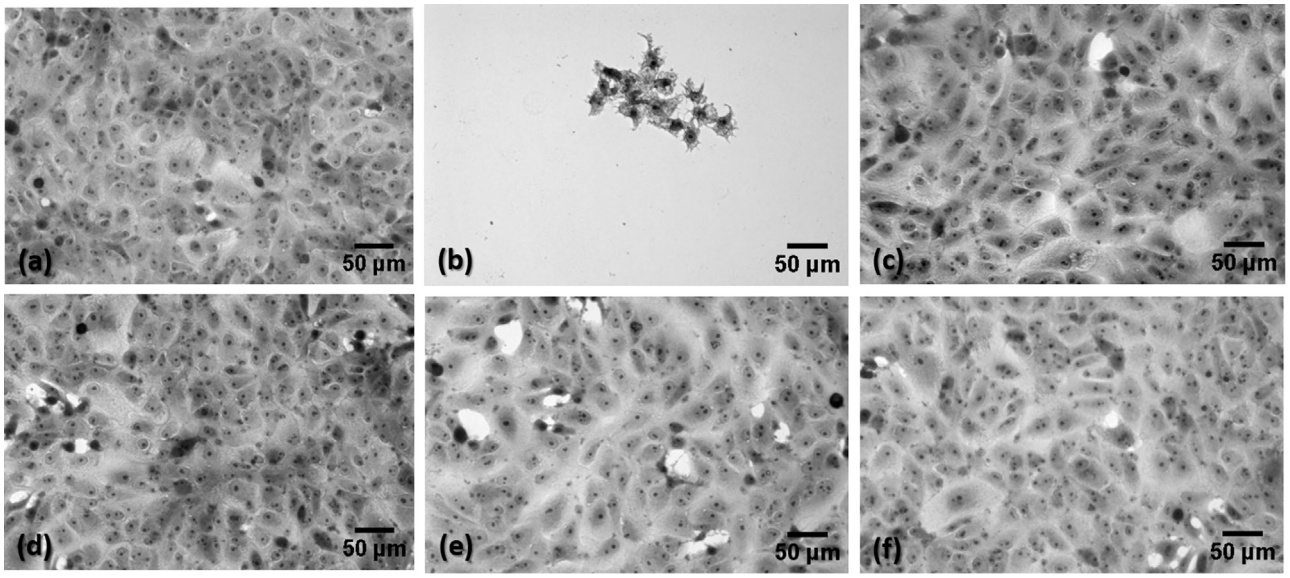

Fig. 8. Observation of Vero cells after staining with toluidine blue in cytotoxicity assay. (a) Negative control, (b) Positive control, (c) GC 40Ca sintered at 1000 °C, (d) GC 30Ca sintered at 1000 °C, (e) GC 20Ca sintered at 900 °C and (f) GC 20CaII sintered at 850 °C.

increased sintering window [25–28], specially to obtain bodies that could be sintered into 3D constructs (scaffolds) [29]. Recently, highly porous wollastonite–diopside ceramics were synthesized using 20CaII glass powders as additional fillers in silicone-based mixtures. The introduction of 20CaII glass particles as secondary fillers enabled us to obtain bioactive crack-free foams with a crushing strength of 6 MPa and 72% of open porosity [30,31].

Regarding crystallization, the addition of MgO in glass compositions allows the formation of diopside in GCs 30Ca, 20Ca and 20CaII (Fig. 4). GC 20CaII presents a higher content of MgO (12 mol%) and Na_2O (9 mol%) (see Table 1), allowing the formation of the combeite phase (PDF # 78–1649).

Fig. 6 shows a SEM micrograph of an acid etched surface of the GCs. GC 40Ca sintered at 1000 °C (Fig. 6a)) has an average crystal size under 5 μm and a small vitreous phase (Table 2). The presence of a larger number of crystals under 5 μm was the key to the development of a material with good flexural strength (98 ± 6 MPa) (Table 3). GC 30 Ca sintered at 1000 °C and GC 20Ca sintered at 900 °C present a high content in the vitreous phase, as seen in Table 3 (37% and 36%, respectively), which may be responsible for the lower flexural strength (64 ± 3 and 74 ± 6, respectively) of these GCs compared to GC 40Ca and GC 20CaII (98 MPa). The flexural strength obtained for GC 20CaII sintered at 850 °C (98 ± 7) was similar to the value obtained for GC 40Ca (Table 3), despite the porosity (9 ± 1) and large crystals up to 20 μm (Fig. 6d)). Cerabone® (Fig. 6(e)) presents a fine microstructure, with crystals under 1 μm uniformly distributed. It is extremely important to note that the crystalline phases contribute both to the strength and the bioactivity, whilst the glassy phase may contribute to the surface activity [32].

The bioactivity behavior of the obtained GCs, shown in Fig. 7, can be explained by the chemical composition of the base glass and by the crystalline phases present in these GCs. As can be seen in Table 1, 20CaII glass has 22 mol% in CaO and is Al_2O_3 and ZrO_2 free. Studies demonstrate that the presence of Al_2O_3 and ZrO_2 in a bioglass tends to decrease its bioactivity, even make it inert, as well as the addition of large quantities of CaO in the composition [33–35]. Regarding the crystalline phases, the presence of wollastonite and/or diopside in GC 40Ca, GC 30Ca and GC 20Ca, as shown in Fig. 4(a), (b) and (c) respectively, was not enough to ensure the bioactivity of these samples (Fig. 7). Some studies reported that these crystalline phases are bioactive [2,3]. However, we found that when diopside and wolastonite are formed in glasses which have components that increase the chemical durability, such as Al_2O_3, ZrO_2 and a high content of CaO (40 mol%), the bioactivity is affected.

As shown in Figs. 7 and 8, reasonable bioactivity was only achieved by GC 20CaII (that is zirconia and alumina free) having combeite ($Na_{4.2}Ca_{2.8}(Si_6O_{18})$) as the main crystalline phase (Fig. 4d)). Combeite has a higher dissolution rate in SBF compared to wollastonite ($CaO.SiO_2$) and diopside ($MgO.CaO.SiO_4$). Stoichiometric combeite ($Na_2Ca_2Si_3O_9$) was previously related as a crystal phase having high bioactivity, in which the onset time to HCA formation in SBF solution was about 33 h [23].

5. Conclusions

In this paper, we developed a new bioactive CaO-MgO-SiO_2-Na_2O-Li_2O glass-ceramic by sintering and simultaneous crystallization of a glass powder compact. Four glass compositions were designed and evaluated concerning densification, bioactivity and mechanical properties. We found that, as expected, additions of Al_2O_3 or ZrO_2 or high contents of CaO (~ 40 mol%) increased the sinterability but are forbidden when bioactivity is desired. The addition of Na_2O reduced the glass transition temperature (T_g), sintering temperature (T_{sint}) and enhanced the sintering window, however it led to degassing during crystallization, resulting in porous materials.

The most bioactive GC developed here, GC 20CaII - 850 °C, shows three crystalline phases (diopside, wollastonite and combeite), approximately 20%vol. of residual vitreous phase, reasonable sinterability (residual porosity < 10%), bending strength ~100 MPa, it is not cytotoxic and, especially, has a significant in vitro bioactivity (3 days to form HCA). This favorable combination of properties suggests that this new GC is a candidate for bone graft implants and warrants further testing.

Acknowledgements

The authors acknowledge Prof. Dr. Oscar Peitl for his valuable experimental support. This work was generously supported by the São Paulo Research Foundation (FAPESP) from São Paulo, Brazil, under the grant numbers 2007/08179-9, 2010/15635-3, 2010/18947-6, 2011/22936-2, 2012/03072-0 and 2013/07793-6 (CEPID).

References

[1] T. Kokubo, S. Ito, S. Sakka, M. Shigematsu, T. Yamamuro, Formation of a high-strength bioactive glass-ceramic in the system $MgO-CaO-SiO_2-P_2O_5$, J. Mater. Sc. 21 (1986) 536–540.
[2] P.N. De Aza, F. Guitian, S. De Aza, Bioeutectic: a new bioactive material for human bone replacement, Biomaterials 18 (1997) 1285–1291.
[3] M.A. Sainz, P. Pena, S. Serena, A. Caballero, Influence of design on bioactivity of novel $CaSiO_3$-$CaMg(SiO_3)_2$ bioceramics: in vitro simulated body fluid test and thermodynamic simulation, Acta Biomater. 6 (2010) 2797–2807.
[4] T. Kokubo, Bioactive glass ceramics: properties and applications, Biomater 12 (1991) 155–163.
[5] V.O. Soares, G.R. Paula, O. Peitl Filho, E.D. Zanotto, Effect of ion exchange on the sinter - crystallisation of low expansion $Li_2O.Al_2O_3.SiO_2$ glass-ceramics, Glass Technol. 52 (2011) 54–56.
[6] D. Shi, Biomaterials and Tissue Engineering, Springer, Berlim, 2004.
[7] T. Kokubo, A/W glass-ceramic: processing and properties, in: L.L. Hench, J. Wilson (Eds.), An Introduction to Bioceramics, 1st ed., World Scientific, Singapore, 1993, pp. 75–88.
[8] O. Peitl Filho, E.D. Zanotto, F.C. Serbena, L.L. Hench, Bioactive glass-ceramics for load-bearing applications, in: L.L. Hench (Ed.), An Introduction to Bioceramics, 2nd ed., Imperial College Press, Singapore, 2013, pp. 495–504.
[9] R. Müller, E.D. Zanotto, V.M. Fokin, Surface crystallization of silicate glasses: nucleation sites and kinetics, J. Non-Cryst. Solids 274 (1–3) (2000) 208–231.
[10] V.O. Soares, R.M.C.V. Reis, E.D. Zanotto, M.J. Pascual, A. Duran, Non-isothermal sinter-crystallization of jagged $Li_2O.Al_2O_3.SiO_2$ glass and simulation using a modified form of the *Clusters* model, J. Non-Cryst. Solids 358 (2012) 3234–3242.
[11] V.O. Soares, O. Peitl, E.D. Zanotto, New sintered Li_2O–Al_2O_3–SiO_2 ultra-low expansion glass-ceramic, J. Am. Ceram. Soc. 96 (4) (2013) 1143–1149.
[12] M.O. Prado, E.D. Zanotto, Glass sintering with concurrent crystallization, Comptes Rendus Chim. 5 (2002) 773–786.
[13] T.J. Clark, S.J. Reed, Kinetics Process involved in the sintering and crystallization of glass powder, J. Am. Ceram. Soc. 69 (11) (1986) 837–846.
[14] J.M.F. Navarro, El Vidrio, 3rd ed., Artegraf, Madrid, 2003, p. 339.
[15] R. Karell, J. Kraxner, M. Chromčíková, M. Liška, Properties of selected zirconia containing silicate glasses II, Ceram. − Silikáty 51 (3) (2007) 125–130.
[16] X. Lu, L. Deng, J. Du, Effect of ZrO_2 on the structure and properties of soda-lime silicate glasses from molecular dynamics simulations, J. Non-Cryst. Solids 491 (2018) 141–150.
[17] S. Krimm, A.V. Tobolsky, Quantitative X-ray studies of order in amorphous and crystalline polymers. Quantitative X-ray determination of crystallinity in polyethylene, J. Polym. Sci. 7 (1951) 57–76.
[18] J.K.M.F. Daguano, C. Santos, M.H.F.V. Fernandes, S.O. Rogero, K. Strecker, Effect of partial crystallization on the mechanical properties and cytotoxicity of bioactive glass from the $3CaO.P_2O_5$-SiO_2-MgO system, J. Mech. Behav. Biomed. Mater. 14 (2012) 78–88.
[19] W.C. Oliver, G.M. Pharr, An improved technique for determining hardness and elastic modulus using load and displacement sensing indentation experiments, J. Mater. Res. 7 (1992) 1564–1583.
[20] ISO DOCUMENT 10993-5. Biological evaluation of medical devices, Part 5, Tests for cytotoxicity: in vitro methods, 1992.
[21] T. Kokubo, H. Takadama, How useful is SBF in predicting in vivo bone bioactivity? Biomater 27 (2006) 2907–2915.
[22] ISO DOCUMENT 10993-5 Biological evaluation of medical devices, Part 5 Tests Cytotox.: Vitr. Methods 1992.
[23] O. Peitl, E.D. Zanotto, L.L. Hench, Highly bioactive P_2O_5-Na_2O-CaO-SiO_2 glass-ceramic, J. Non-Cryst. Solids 292 (2001) 115–126.
[24] D.S. Brauer, R.M. Wilson, T. Kasuga, Multicomponent phosphate invert glasses with improved processing, J. Non-Cryst. Solids 358 (2012) 1720–1723.
[25] M.D. O'Donnell, R.G. Hill, Influence of strontium and the importance of glass chemistry and structure when designing bioactive glasses for bone regeneration, Acta Biomater. 6 (2010) 2382–2385.
[26] F. Baino, M. Ferraris, O. Bretcanu, E. Verne, C. Vitale-Brovarone, Optimization of composition, structure and mechanical strength of bioactive 3-D glass-ceramic

scaffolds for bone substitution, J. Biomater. Appl. 27 (2013) 872–890.
[27] D. Bellucci, A. Sola, A. Anesi, R. Salvatori, L. Chiarini, V. Cannillo, Bioactive glass/hydroxyapatite composites: mechanical properties and biological evaluation, Mater. Sci. Eng. C. 51 (2015) 196–205.
[28] D. Bellucci, V. Cannillo, A novel bioactive glass containing strontium and magnesium with ultrahigh crystallization temperature, Mater. Lett. 213 (2018) 67–70.
[29] A. Nommeots-Nomm, S. Labbaf, A. Devlin, N. Todd, et al., Highly degradable porous melt-derived bioactive glass foam scaffolds for bone regeneration, Acta Biomater. 57 (2017) 449–461.
[30] A.C. Juraski, A.C.D. Rodas, H. Elsayed, E. Bernardo, V.O. Soares, J.K.M.B. Daguano, The in nitro bioactivity, degradation, and cytotoxicity of polymer-derived Wollastonite-Diopside glass-ceramics (425), Mater 10 (4) (2017) 1–19.
[31] L. Fiocco, H. Elsayeda, J.K.M.F. Daguano, V.O. Soares, E. Bernardo, Silicone resinsmixed with active oxide fillers and Ca–Mg Silicate glass as alternative/integrative precursors for wollastonite–diopside glass-ceramic foams, J. Non-Cryst. Solids 416 (2015) 44–49.
[32] D.-M. LIU, Bioactive glass-ceramic: formation, characterization and bioactivity, Mater. Chem. Phys. 36 (1994) 294–303.
[33] O. Jeznach, M. Gajc, K. Korzeb, et al., New calcium-free Na_2O–Al_2O_3–P_2O_5 bioactive glasses with potential applications in bone tissue engineering, J. Am. Ceram. Soc. 101 (2018) 602–611.
[34] A. Hoppe, N.S. Güldal, A.R. Boccaccini, A review of the biological response to ionic dissolution products from bioactive glasses and glass-ceramics, Biomater 32 (2011) 2757–2774.
[35] S.M. Rabiee, N. Nazparvar, M. Azizian, D. Vashaee, L. Tayebi, Effect of ion substitution on properties of bioactive glasses: a review, Ceram. Int. 41 (2015) 7241–7251.